A&A 647, A193 (2021)
https://doi.org/10.1051/0004-6361/202040019

Astronomy & Astrophysics

Apertif view of the OH megamaser IRAS 10597+5926: OH 18 cm satellite lines in wide-area H I surveys

K. M. Hess[1,2], H. Roberts[3], H. Dénes[1], B. Adebahr[4], J. Darling[3], E. A. K. Adams[1,2], W. J. G. de Blok[1,5,2], A. Kutkin[1,6], D. M. Lucero[7], R. Morganti[1,2], V. A. Moss[8,9,1], T. A. Oosterloo[1,2], R. Schulz[1], J. M. van der Hulst[2], A. H. W. M. Coolen[1], S. Damstra[1], M. Ivashina[10], G. M. Loose[1], Y. Maan[1,11], Á. Mika[1], H. Mulder[1], M. J. Norden[1], L. C. Oostrum[1,11], M. Ruiter[1], J. van Leeuwen[1,11], N. J. Vermaas[1], D. Vohl[1], S. J. Wijnholds[1], and J. Ziemke[1,12]

[1] ASTRON, the Netherlands Institute for Radio Astronomy, Postbus 2, 7990 AA Dwingeloo, The Netherlands
e-mail: hess@astron.nl
[2] Kapteyn Astronomical Institute, University of Groningen, PO Box 800, 9700 AV Groningen, The Netherlands
[3] Center for Astrophysics and Space Astronomy, Department of Astrophysical and Planetary Sciences, University of Colorado, 389 UCB, Boulder, CO 80309, USA
[4] Ruhr University Bochum, Faculty of Physics and Astronomy, Astronomical Institute (AIRUB), Universitätsstrasse 150, 44780 Bochum, Germany
[5] Dept. of Astronomy, Univ. of Cape Town, Private Bag X3, Rondebosch 7701, South Africa
[6] Astro Space Center of Lebedev Physical Institute, Profsoyuznaya Str. 84/32, 117997 Moscow, Russia
[7] Department of Physics, Virginia Polytechnic Institute and State University, 50 West Campus Drive, Blacksburg, VA 24061, USA
[8] CSIRO Astronomy and Space Science, Australia Telescope National Facility, PO Box 76, Epping, NSW 1710, Australia
[9] Sydney Institute for Astronomy, School of Physics, University of Sydney, Sydney, New South Wales 2006, Australia
[10] Dept. of Electrical Engineering, Chalmers University of Technology, Gothenburg, Sweden
[11] Anton Pannekoek Institute, University of Amsterdam, Postbus 94249, 1090 GE Amsterdam, The Netherlands
[12] Rijksuniversiteit Groningen Center for Information Technology, PO Box 11044, 9700 CA Groningen, The Netherlands

Received 30 November 2020 / Accepted 13 January 2021

ABSTRACT

We present the serendipitous detection of the two main OH maser lines at 1667 and 1665 MHz associated with IRAS 10597+5926 at $z_{\odot} = 0.19612$ in the untargeted Apertif Wide-area Extragalactic imaging Survey (AWES), and the subsequent measurement of the OH 1612 MHz satellite line in the same source. With a total OH luminosity of $\log(L/L_{\odot}) = 3.90 \pm 0.03$, IRAS 10597+5926 is the fourth brightest OH megamaser (OHM) known. We measure a lower limit for the 1667/1612 ratio of $R_{1612} > 45.9$, which is the highest limiting ratio measured for the 1612 MHz OH satellite line to date. OH satellite line measurements provide a potentially valuable constraint by which to compare detailed models of OH maser pumping mechanisms. Optical imaging shows that the galaxy is likely a late-stage merger. Based on published infrared and far ultraviolet fluxes, we find that the galaxy is an ultra-luminous infrared galaxy (ULIRG) with $\log(L_{\rm TIR}/L_{\odot}) = 12.24$ that is undergoing a starburst with an estimated star formation rate of $179 \pm 40\, M_{\odot}\,{\rm yr}^{-1}$. These host galaxy properties are consistent with the physical conditions responsible for very bright OHM emission. Finally, we provide an update on the predicted number of OH masers that may be found in AWES and estimate the total number of OH masers that will be detected in each of the individual main and satellite OH 18 cm lines.

Key words. masers – galaxies: groups: individual: IRAS 10597+5926 – radio lines: galaxies – galaxies: ISM – galaxies: interactions – galaxies: starburst

1. Introduction

Despite their first discovery nearly four decades ago (Baan et al. 1982), extragalactic OH masers are still relatively rare objects. The majority are a million times more luminous than Galactic OH masers, earning them the name megamasers. It was recognized early on that OH megamasers (OHMs) are well correlated with far-IR luminosity, which is a signpost for the maser pumping mechanism (e.g., Baan 1999): OHMs are essentially always found in luminous or ultra-luminous infrared galaxies ([U]LIRG; Zhang et al. 2014), and they are associated with galaxy mergers, intense nuclear star formation activity (Henkel et al. 1991; Skinner et al. 1997), and regions of dense gas (Darling 2007). The strong correlation of OHMs with galaxy mergers and the redshift information that comes automatically from a detection make them a valuable tracer of the merger history of the Universe and thus a test of hierarchical galaxy evolution models (e.g., Lo 2005; McKean & Roy 2009).

The majority of extragalactic OH masers have been found through the detection of the 1667 MHz line by targeting bright IRAS sources with single dish radio telescopes (e.g., NRAO 300 FT, Baan et al. 1992a; Parkes Observatory, Staveley-Smith et al. 1992; Norris et al. 1989; Arecibo Observatory, Darling & Giovanelli 2002; Fernandez et al. 2010; Green Bank Telescope; GBT, Willett 2012). Only of order a dozen OHMs have been studied at greater than arcsecond resolution. Those that have been studied show that the maser emission is confined within a 100 pc region of the nucleus. Up to 30% of the emission may be diffuse within the 100 pc region, while the majority of the emission is found in compact regions ∼10 pc in size (Lo 2005, and sources therein).

In fact, at radio frequencies, OH has two main lines at 1665 and 1667 MHz and two satellite lines at 1612 and 1720 MHz (Radford 1964). Extragalactic OHMs exhibit a broad range of 1667/1665 hyperfine ratios (from $R_H < 1$ to $R_H > 10$) with an

average close to $R_H \sim 5$ (McBride et al. 2013). The variation observed in this property has been successfully modeled as a combination of a clumpy maser medium of overlapping clouds (Parra et al. 2005) and far-IR line overlap, with pumping primarily occurring through the 53 μm line (Lockett & Elitzur 2008). The former explains how compact masers (with typically high R_H values) appear embedded in a diffuse emission (with low R_H) in high resolution very long baseline interferometry (VLBI) observations (Lonsdale 2002). Together, these models account for how warmer dust is correlated with higher IR luminosities (Willett et al. 2011; Lockett & Elitzur 2008).

However, very little is known about the ratio between main and satellite lines in OHMs. In local thermodynamic equilibrium (LTE), the emission line ratios are expected to be 1:5:9:1 for 1612:1665:1667:1720 MHz. Measuring the ratio of satellite to main lines provides a test for complex maser pumping models that predict the 1667/1612 (R_{1612}) and 1667/1720 (R_{1720}) ratios based on the variation in the optical depth of the 1667 MHz line and the assumption that all lines have the same excitation temperature (Lockett & Elitzur 2008; McBride et al. 2013, see also Willett et al. 2011). There are only four extragalactic detections of 1612 MHz in emission, which is a requirement to measure the 1667/1612 line ratio: Arp 220 (Baan & Haschick 1987), Arp 299/IC 694 and Mrk 231 (Baan et al. 1992a), and IRAS F15107+0724 (McBride et al. 2013). (A tentative detection of II Zw 96/IRAS 20550+1655 by Baan et al. 1989 was refuted by McBride et al. 2013.) Their corresponding measurements of the 1667/1612 ratio span $R_{1612} \sim 7-29$ over a relatively narrow range in 1667 MHz optical depth (Baan et al. 1992a; McBride et al. 2013). In addition, M 82 is detected with a complex mix of 1612 MHz emission and absorption (Seaquist et al. 1997), and three extragalactic OH masing sources have been detected in 1612 MHz absorption: NGC 253 (Frayer et al. 1998), PKS 1413+135 (Darling 2004), and PMN J0134−0931 (Kanekar et al. 2005). In all of the cases when 1612 MHz is detected in absorption, the 1720 MHz line is found in conjugate emission. In contrast, while Arp 220 is detected in 1612 MHz emission, the 1720 MHz line is seen in absorption (Baan & Haschick 1987). These complex cases have not yet been captured in the discussion of the maser pumping models.

In addition to probing the state of the masing gas, satellite lines of OH are used to measure the universality of fundamental constants at high redshift (Varshalovich & Potekhin 1995; Darling 2003; Chengalur & Kanekar 2003). The four OH lines have different dependencies on the fine structure constant, $\alpha = e^2/\hbar c$, the electron-proton mass ratio, $\mu = m_e/m_p$, and the proton gyromagnetic ratio, g_p (Kanekar et al. 2005). Early quasar studies claimed a possible changing α (e.g., Webb et al. 2001). While no evidence for changing fundamental constants has been found to date from centimeter lines, only two OH sources are known, which have been used for such studies (PKS 1413+135, $z = 0.24671$; PMN J0134−0931, $z = 0.765$; Darling 2004; Kanekar et al. 2012, 2018), as have a small number of sources using other lines (e.g., ammonia, Flambaum & Kozlov 2007; or methanol, Jansen et al. 2011).

Large-volume radio spectral line surveys at 1.4 GHz, typically aimed at targeting the 21 cm line of neutral hydrogen, H I, provide an unprecedented opportunity to discover and study the rare, but cosmologically important, extragalactic OHMs (e.g., Briggs 1998; Suess et al. 2016). The large bandwidth of new and upgraded instruments undertaking these surveys will allow the simultaneous measurement of main and satellite lines, while also detecting or putting limits on the H I emission and absorption strength (Gupta et al. 2020). Apertif is one of these upgraded survey machines: a new phased array feed (PAF) instrument on the Westerbork Synthesis Radio Telescope undertaking commensurate spectral line, continuum, and polarization surveys in the frequency range 1130–1430 MHz (Adams & van Leeuwen 2019; van Capellen et al., in prep.; Hess et al., in prep.). In addition to directly detecting H I in galaxies out to $z \sim 0.07$ (and through H I stacking or absorption out to the bandwidth limit, $z \sim 0.2$), the observations are capable of detecting extragalactic OH masers where the 1667 MHz line has been redshifted to $0.166 < z < 0.476$.

In this paper, we present the untargeted, serendipitous detection of IRAS 10597+5926 in both the 1667 and 1665 main lines, as well as a measurement of the 1612 MHz satellite line with an integrated signal-to-noise ratio (S/N) of 2.2σ, which we treat as an upper limit. We use published IR and far ultraviolet (FUV) fluxes available in the NASA/IPAC Extragalactic Database (NED)[1] to calculate the host galaxy properties, including the star formation rate (SFR) and stellar mass, and confirm that IRAS 10597+5926 is an ultra-luminous infrared galaxy (ULIRG). The 1612 MHz emission measurement is the highest 1667/1612 ratio lower limit measured to date and the most stringent constraint on existing maser pumping models. This measurement demonstrates the power of upcoming untargeted, large-volume H I surveys, where the broad bandwidth is valuable for simultaneously observing multiple OH lines either directly or through the potential of OH stacking. The detection of IRAS 10597+5926 also showcases the automated source finding and visual inspection tools under development that make discoveries within these surveys, as well as the harvesting of data from spectral line sources, possible.

Throughout this paper, we assume a ΛCDM cosmology with $H_0 = 70$ km s^{-1} Mpc^{-1}, $\Omega_M = 0.27$, and $\Omega_\Lambda = 0.73$.

2. Apertif data

2.1. Data reduction, imaging, and source finding

The area of sky containing IRAS 10597+5926 was observed in October 2019 (ObsId 191003042) as part of the ongoing Apertif Wide-area Extragalactic imaging Survey (AWES). The Apertif spectral line, continuum, and polarization surveys will be described in detail in Hess et al (in prep.). In short, Apertif is a PAF instrument upgrade to the Westerbork Synthesis Radio Telescope, which increases the field-of-view to 6.4–8 deg^2 and the spectral bandwidth to 300 MHz from 1130–1430 MHz. Every AWES survey pointing is observed for 11.5 hours. The data are reduced through an automated data reduction pipeline called *Apercal* (Schulz et al. 2020; Adebahr et al., in prep.), which produces: cleaned multi-frequency continuum (Stokes *I*) images; polarization (Stokes *V*) images and (Stokes *Q*- and *U*-) cubes; and continuum-subtracted spectral line dirty image cubes with 12.2–36.6 kHz resolution. The raw, calibrated, and imaged data from the first 12 months of observing (1 July 2019–30 June 2020) are publicly available as part of the first Apertif data release[2] (Apertif DR1; Adams et al., in prep.).

As part of ongoing Apertif work toward developing a catalog of H I spectral line sources, the data were run through a spectral line source finding pipeline. The pipeline is still under development and will be described in a future paper. In short, we used

[1] http://ned.ipac.caltech.edu; The NASA/IPAC Extragalactic Database (NED) is funded by the National Aeronautics and Space Administration and operated by the California Institute of Technology.
[2] Persistent identifier (PID): http://hdl.handle.net/21.12136/B014022C-978B-40F6-96C6-1A3B1F4A3DB0

a well-tested software application, SoFiA[3] (Serra et al. 2015), to find candidate spectral line sources. SoFiA finds sources by searching for emission at multiple angular and velocity resolutions after smoothing the data cube with 3D kernels that are specified by the user. At each resolution, voxels are detected if their absolute value is above a threshold given by the user (in units of the rms noise). The final 3D mask is the union of the 3D masks that are constructed at the various resolutions. Objects are cleaned to 0.5σ within the masks, defined by SoFiA, that encompass the source. The data cubes are compound beam-corrected using standard tasks in the Miriad software package (Sault et al. 1995, 2011) and adjusted to the NRAO VLA Sky Survey (NVSS) flux scale (see documentation in the Apertif data release). Final data products, which include moment maps and spectrum plots, are created using Astropy v2.0 (Astropy Collaboration 2018). The final data products are then inspected by eye, and unusual objects are flagged for potential science interest.

In the context of OH masers, the 300 MHz frequency range covered by the Apertif surveys provides a window to observe the 1667 MHz line between redshifts of $0.16599 < z < 0.47554$. This redshifted OH maser line can effectively masquerade as an H I source in the nearby Universe, as it has similar flux densities and line widths (e.g., Briggs 1998; Suess et al. 2016; Haynes et al. 2018). A spectral line source finding pipeline works effectively for both H I and OH lines because it cannot distinguish between the two. In this way, we serendipitously detected the 1667 MHz line of IRAS 10597+5926 (J2000 11:02:46.9+59:10:37), redshifted to $z_\odot = 0.19612$, while inspecting candidate H I detections. In this case, the OH nature of the source was clear because the 1665 MHz line was also clearly detected. A literature search found that the 1667 MHz line was presented in an unrefereed IAU Conference Proceedings by Willett (2012), but the 1665 MHz line was not discussed and may have been left unreported due to a poorly determined or perhaps over-subtracted baseline.

We note that, unfortunately, frequencies below ~1300 MHz, corresponding to the lower half of the Apertif band, are strongly impacted by radio frequency interference (RFI) from satellites. As a result, Apertif data are to date only processed between 1430–1280 MHz, decreasing the effective available redshift range to $0.16599 < z < 0.30262$ for OH line detections. Table 1 lists the redshift range in which each of the OH maser lines is visible to Apertif.

2.2. Post-processing

In the field of IRAS 10597+5926, there are two bright continuum sources at roughly 770 ± 15 mJy (20 arcseconds away) and 580 ± 10 mJy (30 arcseconds away) that are not perfectly modeled by the calibration in the *Apercal* pipeline, leaving faint concentric rings around the continuum sources. These rings vary slowly in frequency and are faintly evident even in the line cubes. To remove the artifacts, we masked the OH maser source and refit the baseline at every spatial pixel in the cubes with a five-knot natural cubic spline[4] along the frequency axis. The line cubes consist of 1216 channels of approximately 7 km s^{-1}; as such, a spline segment spans more than 1700 km s^{-1}, ensuring that every spline segment is dominated by emission-free channels. The resulting data cube has a noise of 1.27 mJy beam^{-1}.

The source finding pipeline was then rerun on the new data cube, which identified the 1667 MHz and 1665 MHz emission as separate line sources. For the subsequent analysis, we extracted a pixel spectrum at the location of the 1667 MHz peak in the total intensity map. The spectrum was then boxcar-smoothed by three channels (top panel of Fig. 1). For the redshift of the system, we took the line center calculated by SoFiA for the 1667 MHz line and used it to calculate the expected frequencies for the 1665 MHz and 1612 MHz lines. To calculate the line flux, we integrated the pixel spectrum over ±27 channels (433 km s^{-1}) of the 1667 MHz line center and ±19 channels (308 km s^{-1}) of the 1665 MHz line, which correspond to the widths of the SoFiA masks for each source.

[3] https://github.com/SoFiA-Admin/SoFiA
[4] https://github.com/madrury/basis-expansions/

Table 1. Range of redshifts for OH maser lines visible to Apertif.

OH line	1430 MHz	1280 MHz	1130 MHz
1612 MHz	0.12743	0.25956	0.42675
1665 MHz	0.16462	0.30110	0.47381
1667 MHz	0.16599	0.30262	0.47554
1720 MHz	0.20316	0.34416	0.52259

Notes. Apertif observes frequencies up to 1430 MHz, which defines the low redshift limit of the Apertif bandwidth; 1280 MHz is the redshift upper limit for frequencies that are relatively unimpaired by interference; 1130 MHz is the low frequency (high redshift) limit for the Apertif bandwidth.

2.3. 1612 MHz data

Based on the systemic redshift measured by SoFiA, we calculated that the 1612 MHz satellite line of IRAS 10597+5926 would also fall in the Apertif bandwidth, redshifted to 1347.9469 MHz. We applied the same spline fitting technique to this data cube to remove residual artifacts. The resulting cube has a noise of 1.30 mJy beam^{-1}. We extracted the pixel spectrum at the position of the peak of the 1667 MHz total intensity map. The spectrum was then boxcar-smoothed by five channels (bottom panel of Fig. 1). To calculate the line flux, we integrated over ±8 channels (138 km s^{-1}) of the expected 1612 MHz line center. This corresponds, subjectively, to a symmetric extent roughly the width of the brightest part of the 1665 and 1667 MHz lines, and where we would expect the 1612 MHz line to be brightest if it is present (see also the gray shaded region in Fig. A.1).

We conducted a number of tests to understand the significance of a measurement at the exact location of the predicted 1612 MHz line, including correlating the Apertif spectrum with different matched filters, and conducting a Bayesian analysis with a strong redshift prior. These tests are described in Appendix A. The matched filter tests modestly strengthen the case for a detection of the 1612 MHz line. However, the Bayesian analysis suggests that there is roughly a one in three chance of a detection at that location given the noise of the spectrum. As a result, we describe our measurement of the integrated flux of the 1612 MHz line as an upper limit.

3. Results

We measured all OH maser emission lines of the $^2\Pi_{3/2}(J = 3/2)$ state that are within in the Apertif bandwidth: the 1612, 1665, and 1667 MHz lines, redshifted to $z_\odot = 0.19612$. The two main lines are clearly visible in the top panel Fig. 1. They have integrated S/Ns of 12 and 57, respectively. The bottom panel of Fig. 1 shows the spectrum and predicted location of the 1612 MHz satellite line. The peak of the spectrum within

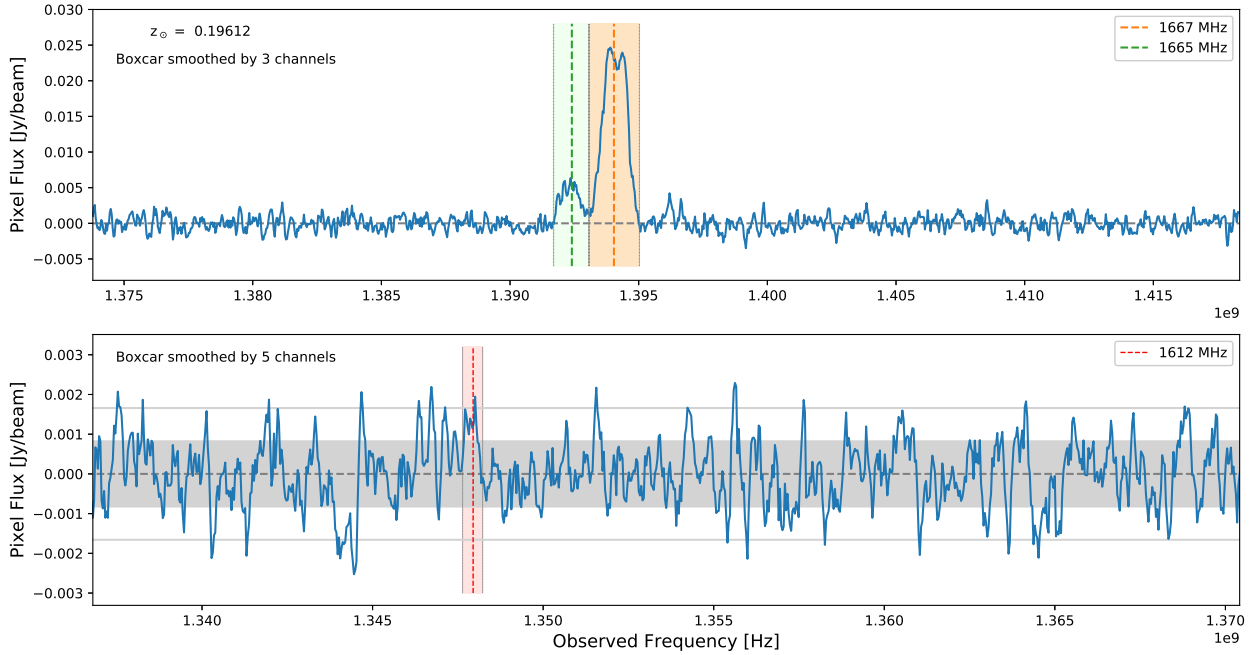

Fig. 1. Pixel spectra extracted at the position of the peak of the 1667 MHz total intensity map. *Top*: spectrum of the 1665 and 1667 MHz main lines. *Bottom*: spectrum of the 1612 MHz satellite line. The 1667 MHz line center is provided by a fit to the line profile by SoFiA. The 1665 and 1612 MHz lines are plotted at the expected frequency based on the 1667 MHz line redshift. The orange, green, and red shaded regions indicate the channel range used to calculate the integrated flux of each line, which correspond to widths of 433, 308, and 138 km s^{-1}, respectively. The gray shaded region in the bottom plot shows the ±1 sigma noise range of the smoothed data; the gray line indicates ±2 sigma.

the estimated profile width is measured to be 2.3 sigma above the noise, while the integrated line profile over the same width has an S/N of 2.2. The calculations of the integrated S/Ns take into account the correlated noise due to the smoothing of the spectra. Only the 1720 MHz satellite line remains outside the frequency range of Apertif at 1438 MHz.

Given our chosen cosmology, IRAS 10597+5926 sits at a luminosity distance of D_L = 963 Mpc. Assuming isotropic emission, we measure the luminosity in the 1667 and 1665 MHz lines to be $\log(L/L_\odot) = 3.83 \pm 0.01$ and 3.09 ± 0.04, respectively, and determine a 1612 MHz upper limit of $\log(L/L_\odot) \leq 2.2 \pm 0.2$. Our errors reflect the uncertainty in the flux measurements based on the noise in the spectra. The total luminosity in the 1665 and 1667 lines, $\log(L/L_\odot) = 3.90 \pm 0.03$, makes IRAS 10597+5926 the fourth most luminous OH maser source known and places it on the margin of classification as an OH gigamaser. Our flux seems to be in good agreement with that of Willett (2012), who measure $\log(L/L_\odot) = 3.85$ for the 1667 MHz line using the GBT, although the cosmological parameters used to calculate their value have not been published.

Figure 2 shows an optical PanSTARRS[5] (Chambers et al. 2016) g-band image with the Apertif 1.36 GHz radio continuum contours. The radio continuum image has an rms of 33 μJy beam^{-1} at the location of IRAS 10597+5926, and the continuum source associated with the maser is a 6 ± 1 mJy point source at the resolution of Apertif, 13 × 17 arcsec. The ground-based images show a disturbed optical morphology that we interpret as an advanced merger, as is seen in a majority of ULIRG sources for which there is sufficient imaging (e.g., Clements et al. 1996; Farrah et al. 2001).

Among powerful OHMs, IRAS 10597+5926 is unique in that the 1667 and 1665 MHz lines are relatively narrow and distinct, whereas the brightest gigamasers show blended

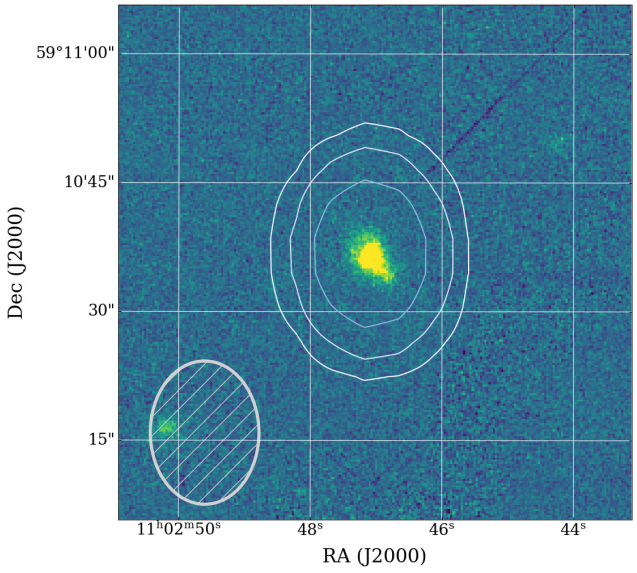

Fig. 2. Continuum contours 6, 12, and 24 × 10^{-4} Jy beam^{-1} on a PanSTARRS g-band image. The radio source is unresolved by the 13 × 17 arcsec beam of Apertif (hatched gray ellipse in the bottom left corner). The continuum image has a noise of 33 μJy beam^{-1}. The disturbed optical appearance is consistent with the galaxy in the late stages of a merger.

emission features for the 1667 and 1665 MHz lines spanning over 1000 km s^{-1} (Staveley-Smith et al. 1989; Baan et al. 1992b; Darling & Giovanelli 2001). The brightest known OHM, IRAS 14070+0525, spans 2400 km s^{-1}. Baan et al. (1992b) suggests that this is the result of a violent merger, an active galactic nucleus outflow, or a 500 km s^{-1} rotating disk around a supermassive black hole in which the 1667 and 1665 lines are

[5] https://panstarrs.stsci.edu/

blended (Baan & Klöckner 2001). We note that the 1667 MHz line appears to have two distinct peaks; however, VLBI imaging is required to determine anything about the configuration of the masing material or the narrowness of the OH lines in IRAS 10597+5926.

4. Discussion

This first OHM detected, serendipitously, from the Apertif survey AWES demonstrates that future wide-area H I surveys will not just be a useful way to discover new extragalactic OH masers (Briggs 1998): with their broad spectral bandwidth, they will also provide simultaneous detections or constraints on OH satellite lines. Below, we present the host galaxy properties, we discuss the properties of the OHM in the context of what is known about satellite lines, and we present a prediction for the discovery space that will be revealed with AWES.

4.1. Host galaxy properties

The IR luminosity and SFR of the host galaxy are tied to the physical conditions thought to be responsible for OHM activity. IRAS 10597+5926 is a very luminous OHM, so one would expect it to be very luminous in the mid- and far-IR. We used publicly available archival data to confirm the extreme IR and SFR properties of this system.

IRAS 10597+5926 is detected in FUV by GALEX (Buat et al. 2007), in all four WISE IR band images at 3.4, 4.6, 12, and 22 μm (Zhang et al. 2014), and in IRAS 60 and 100 μm band images (Moshir 1990). For the WISE bands, we used k-corrected fluxes based on a galaxy template and spectral energy distribution fitting (Jarrett et al. 2019). This is not available for IRAS bands; therefore, for these bands and for the GALEX data we took into account a zeroth order k-correction of $1/(1+z)$ dependence with redshift and represented the additional uncertainty in the error.

We estimated the SFR using two methods from independent subsets of the available IR and UV data. First, we calculated the total IR (TIR) flux from IRAS as outlined in Sanders & Mirabel (1996). The IRAS 12 and 25 μm fluxes are upper limits. Ignoring these values, we find a lower limit to be $\log(L_{\rm TIR}/L_\odot) > 12.24$. By including them, we find an upper limit to the TIR luminosity of $\log(L_{\rm TIR}/L_\odot) < 12.37$. In fact, the WISE W3 and W4 fluxes suggest that the 12 and 25 μm contribution may be an order of magnitude lower than that suggested by the abovementioned upper limit. To calculate the SFR, we combined Eqs. (11) and (12) from Kennicutt & Evans (2012)[6] to derive an FUV+IR SFR from the $L_{\rm TIR}$ lower limit of $179 \pm 40\ M_\odot\ {\rm yr}^{-1}$. Alternatively, using the k-corrected WISE 22 μm band (W4) and calibration from Cluver et al. (2017), we find an SFR of $108 \pm 42\ M_\odot\ {\rm yr}^{-1}$. We note that W4 is a better estimate of SFR than W3 in ULIRGs because of, among other things, strong Si dust absorption in the W3 band (T. Jarrett, priv. comm.). Finally, we estimate a galaxy stellar mass based on the WISE 3.4 μm (W1) and the mass-to-light ratio from Cluver et al. (2014) to be $\log(M_*/M_\odot) = 10.65 \pm 0.14$.

The lower limit to the TIR luminosity, which is calculated exclusively from the 60 and 100 μm far-IR bands, firmly qualifies IRAS 10597+5926 as a ULIRG (Houck et al. 1985). Although we calculated a range of SFRs based on far-IR+FUV or mid-IR, both estimates put the rate at well over $100\ M_\odot\ {\rm yr}^{-1}$, and indeed the WISE 3.4–4.6 μm (W1–W2 = 0.987 ± 0.053) and 4.6–12 μm (W2–W3 = 4.315 ± 0.058) colors place it firmly in the range of starbursting galaxies (Cluver et al. 2014). This is consistent with the physical conditions responsible for OHM activity.

[6] See also Murphy et al. (2011), Hao et al. (2011) for the constants used in these equations.

4.2. OH line ratios

In LTE, the OH lines are expected to have ratios of 1612:1665:1667:1720 = 1:5:9:1 (Radford 1964; Robinson & McGee 1967; Henkel et al. 1991). However, a broad range of values has been measured in megamasers, with the highest resolution images revealing that compact emission tends to have 1667/1665 emission ratios closer to $R_H = 5$ (Lonsdale 2002).

For IRAS 10597+5926, we find (limiting) line ratios of 1:8.3:45.9. This corresponds to a hyperfine ratio between 1667/1665 of $R_H = 5.5 \pm 0.5$. The 1667/1612 ratio, $R_{1612} > 45.9$, is the largest line ratio limit ever measured for this satellite line. Figure 3, adapted from McBride et al. (2013), shows our upper limit (red arrow) versus all existing measurements and limits in the literature[7]. For direct comparison, we also calculated an upper limit (black arrow) based on the methodology of McBride et al. (2013), who used $F_{1612} = \sigma_{1612}\,\Delta\nu_{1667}$, where σ_{1612} is the rms of the 1612 MHz spectrum and $\Delta\nu_{1667}$ is the width of the 1667 MHz line containing 75% of the line emission. For IRAS 10597+5926, $\Delta\nu_{1667}$ is ±13 channels – more than 60% wider than our estimate. The black arrow falls within the uncertainty of our estimate, but we note that this method is (1) independent of the properties of the spectrum at the predicted location of the line and (2) independent of the shape of the 1667 MHz line, which may suggest a more individualized approach. In fact, if we integrate the 1612 MHz spectrum over ±13 channels, we get the same lower limit as that indicated by the red arrow.

The solid black line in Fig. 3 shows the predicted line ratios in "color-color" space if all OH lines in the $^2\Pi_{3/2}(J = 3/2)$ state have equal excitation temperatures (Lockett & Elitzur 2008; McBride et al. 2013). If the R_{1612} ratio deviates from this line, it may indicate that secondary maser pumping mechanisms are important and should be explored in future models. At face value, our measurement is among the strongest constraints indicating that OHMs may still be globally consistent with the equal excitation temperature hypothesis, although a deviation from this is also within the uncertainties of the measurement.

4.3. Updated predictions for Apertif, and a word on 1612 co-detections and stacking

The Apertif surveys have recently been guaranteed observing time through December 2021, for a total of 30 months of survey operations. Previous papers estimated the Apertif OHM 1667 MHz detection rate based on specifications before the surveys were operational (e.g., McKean & Roy 2009). Here, we provide an update on the expected number of detections for AWES based on Roberts et al. (2021).

The estimate combines the OH luminosity function and assumed merger evolution rate with the redshift range, area, and sensitivity of the radio survey. The average OH line has a width of about $150\ {\rm km\,s}^{-1}$, which covers roughly ~23 Apertif channels. We assumed that the data quality is consistent with

[7] We note that the original McBride et al. (2013) plot had two black points despite their table only listing one detection. Ultimately, a wiggle in the spectrum of IRAS 11028+3130 was deemed unreliable and updated in the table as an upper limit, but was accidentally left in the plot (J. McBride, priv. comm.). We have corrected it here.

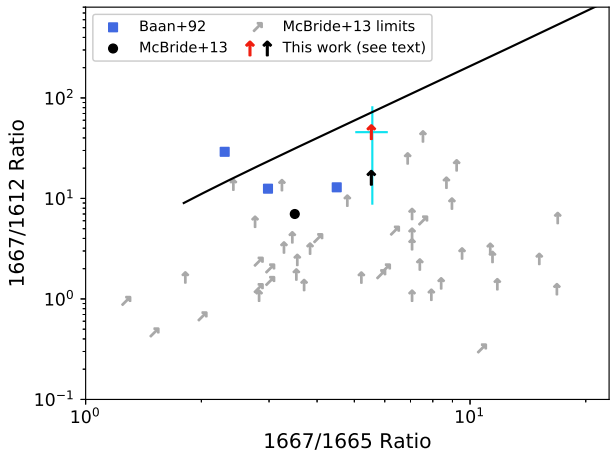

Fig. 3. OH color-color plot for the 1612 MHz line, adapted from McBride et al. (2013). Blue squares come from the literature, collated by Baan et al. (1992a) in their Table 2(a); the black circle and the gray arrows are the detection and upper limits from McBride et al. (2013), respectively. The red arrow is the R_H ratio and R_{1612} upper limit from this work; the cyan cross shows our uncertainties; the black arrow is the upper limit calculated using the McBride et al. (2013) methodology (see Sect. 4.2). The black line shows the predicted ratios assuming equal excitation temperatures for all OH lines, with varying 1667 MHz optical depth (Lockett & Elitzur 2008; McBride et al. 2013).

Apertif DR1, which achieves an average noise of approximately 1.3 mJy beam^{-1} in the H I cubes at 36.6 kHz spectral resolution, and we required the OHMs to be 5σ detections. Though there is much speculation regarding the exact value, we assumed a galaxy merger evolution rate (γ) of 2.2 (Lotz et al. 2011). This value is associated with major mergers, which are the sources of most OHMs.

In addition, an extrapolation of the calculation for the 1667 MHz detections can be done to determine the number of satellite lines that may be detected by Apertif. Assuming all OHMs produce every satellite line and the median line ratios from McBride et al. (2013), we can say that the 1667/1665 line ratio is about 5 and that the 1667/1612 and 1667/1720 ratios are both around 20. This means we need five times more sensitivity for the 1665 MHz line and 20 times more sensitivity to detect 1612 and 1720 MHz lines. Using this and the adjusted redshift ranges (see Table 1), we can predict the number of detections for each line.

The exact survey plan for 2021 is under discussion, so we present the numbers for the survey observing through the end of 2020 as well as two possible strategies for 2021 in Table 2. Column (1) is the frequency of the OH line in megahertz. Column (2) is the assumed line ratio with respect to the 1667 MHz line and is the median line ratio from McBride et al. (2013). Column (3) is the number of OHMs expected from AWES observations in the first 18 months of the survey through the end of 2020, which covers about 1500 deg^2. Column (4) is the total number of OHMs assuming that AWES continues to build up sky coverage in the same way as it did for the previous 18 months, for an estimated coverage of 2500 deg^2. Column (5) assumes that AWES reobserves the existing coverage of approximately 1500 deg^2 to get 1.4 times more sensitivity in spectral line maps. In both future cases, we also estimate the number of OHMs that would be detected between 1430–1530 MHz in 1000–1500 deg^2 assuming the Apertif frequency coverage will shift to avoid RFI beyond 1280 MHz (see caption).

Table 2. OH line detection predictions for AWES to 2020 and beyond.

OH line MHz (1)	Line Ratio [a] (2)	AWES [b] 1500 deg^2 (3)	AWES [b,c] 2500 deg^2 (4)	1.4x AWES [b,c] 1500 deg^2 (5)
1612	20	2^{+1}_{-1}	4^{+1}_{-1}	5^{+1}_{-1}
1665	5	17^{+4}_{-3}	28^{+6}_{-5}	25^{+5}_{-4}
1667	1	76^{+17}_{-13}	127^{+27}_{-21}	103^{+24}_{-19}
1720	20	$0.5^{+0.2}_{-0.2}$	$0.9^{+0.4}_{-0.3}$	2^{+1}_{-1}

Notes. [a]The assumed line ratio is in relation to the primary 1667 MHz line and is the median line ratio from McBride et al. (2013). [b]The numbers of detections are calculated for the frequency range 1280–1430 MHz. [c]For AWES projections beyond 2020 that may shift the frequency coverage (see text), we predict that Apertif will detect an additional ~12–20 (4–6) OHMs in the 1667 (1665) MHz line and an additional ~1–2 OHMs in each of the satellite lines between 1430–1530 MHz, on top of what is listed above.

We estimate the total number of Apertif 1667 MHz OHM detections to be on the order of 110–150 (depending on the 2021 strategy and including a broader frequency range in that 12-month period), increasing the number of known OHMs by over 100%. The large error bars are due to the limited number of known OHMs; as more are discovered, these predictions can be tightened.

This prediction is much higher than the approximately 19 OHMs that have been reported by the Arecibo Legacy Fast ALFA Survey (ALFALFA; Haynes et al. 2018), which covered ~7000 deg^2. However, it is very likely that ALFALFA has yet to discover all potential OHMs, and Suess et al. (2016) present 60 ambiguous sources detected by ALFALFA's 40% data release alone. Furthermore, Apertif's sensitivity is about a factor of two improved over ALFALFA (1.86 mJy beam^{-1} over 48.8 kHz after Hanning smoothing; Haynes et al. 2018): This is an important consideration for detecting OHMs since they must be redshifted, and therefore fainter, to be at the proper frequency for detection.

For undetected 1612 MHz lines, one may attempt to stack OHMs in bins of R_H, redshift, or other physically meaningful parameters. Given the expected number of 1667 MHz detections, and assuming the noise decreases proportional to the square root of the number of objects, we expect that stacking would modestly improve the detection threshold by a factor of a few in each bin.

5. Conclusions

We present the AWES OHM detection of IRAS 10597+5926. The main lines at 1667 and 1665 MHz were found redshifted to $z_\odot$ = 0.19612 by an automated spectral line source finding pipeline. The optical image suggests that IRAS 10597+5926 is a late-stage merger. From IR imaging, we show that the host galaxy is a ULIRG, and estimate a log stellar mass of 10.65±0.14 and an SFR up to 179 ± 40 $M_\odot$ yr^{-1}. We measure the total OH luminosity to $\log(L/L_\odot)$ = 3.90 ± 0.03, putting it on the cusp of the highest luminosity OH sources, OH gigamasers. The extreme SFR and IR luminosity are consistent with the properties of the brightest known OHMs to date.

The untargeted detection by AWES demonstrates the natural ability of wide-area H I surveys with broad frequency bandwidth and complimentary redshift range to benefit spectral line searches for OHMs. We predict that of order 110–150 sources will be found in the AWES survey and speculate that of

order 4–6 OH sources may be detected in satellite lines. This increases the number of both known OHMs and OH satellite lines by more than 100%. The future is bright for OHMs: wide-area H I surveys in addition to AWES, such as WALLABY, are expected to detect more than 100 OHMs over a different area of sky (Koribalski et al. 2020). In fact, Roberts et al. (2021) suggest that WALLABY may find even more OHMs, and, based on our results, WALLABY will detect even more satellite line sources. Meanwhile, dedicated searches in absorption against background radio sources (Apertif SHARP; FLASH, Allison et al. 2020; and MALS, Gupta et al. 2020) will detect OH in different masing environments.

Acknowledgements. We are grateful to Tom Jarrett for providing *k*-corrected WISE magnitudes and additional insight into the IR nature of the source; to James Allison for help in running the FLASHfinder tool to better understand the reliability of our measurements; and to James McBride for advice in recreating Fig. 6b from his paper. We also thank the anonymous referee for their comments which improved the quality of this paper. H.R. and J.D. acknowledge support from the National Science Foundation grant AST-1814648. E.A.K.A. is supported by the WISE research programme, which is financed by the Netherlands Organization for Scientific Research (NWO). J.M.vd.H. acknowledges funding from the European Research Council under the European Union's Seventh Framework Programme (FP/2007-2013)/ERC Grant Agreement No. 291531 ('HIStoryNU'). J.vL. and L.C.O. acknowledge funding from the European Research Council under the European Union's Seventh Framework Programme (FP/2007-2013)/ERC Grant Agreement n. 617199 ('ALERT'), and from Vici research programme 'ARGO' with project number 639.043.815, financed by the Dutch Research Council (NWO). D.V. acknowledges support from the Netherlands eScience Center (NLeSC) under grant ASDI.15.406. This work makes use of data from the Apertif system installed at the Westerbork Synthesis Radio Telescope owned by ASTRON. ASTRON, the Netherlands Institute for Radio Astronomy, is an institute of the Dutch Science Organisation (De Nederlandse Organisatie voor Wetenschappelijk Onderzoek, NWO). This research has made use of the NASA/IPAC Extragalactic Database (NED), which is funded by the National Aeronautics and Space Administration and operated by the California Institute of Technology. The Pan-STARRS1 Surveys (PS1) and the PS1 public science archive have been made possible through contributions by the Institute for Astronomy, the University of Hawaii, the Pan-STARRS Project Office, the Max-Planck Society and its participating institutes, the Max Planck Institute for Astronomy, Heidelberg and the Max Planck Institute for Extraterrestrial Physics, Garching, The Johns Hopkins University, Durham University, the University of Edinburgh, the Queen's University Belfast, the Harvard-Smithsonian Center for Astrophysics, the Las Cumbres Observatory Global Telescope Network Incorporated, the National Central University of Taiwan, the Space Telescope Science Institute, the National Aeronautics and Space Administration under Grant No. NNX08AR22G issued through the Planetary Science Division of the NASA Science Mission Directorate, the National Science Foundation Grant No. AST-1238877, the University of Maryland, Eotvos Lorand University (ELTE), the Los Alamos National Laboratory, and the Gordon and Betty Moore Foundation. This research made use of Astropy, (`http://www.astropy.org`) a community-developed core Python package for Astronomy (Astropy Collaboration 2013, 2018).

References

Adams, E. A. K., & van Leeuwen, J. 2019, Nat. Astron., 3, 188
Allison, J. R., Sadler, E. M., & Whiting, M. T. 2012, PASA, 29, 221
Allison, J. R., Sadler, E. M., & Meekin, A. M. 2014, MNRAS, 440, 696
Allison, J. R., Sadler, E. M., Bellstedt, S., et al. 2020, MNRAS, 494, 3627
Astropy Collaboration (Robitaille, T. P., et al.) 2013, A&A, 558, A33
Astropy Collaboration (Price-Whelan, A. M., et al.) 2018, AJ, 156, 123
Baan, W. A. 1999, in Activity in Galaxies and Related Phenomena, eds. Y. Terzian, E. Khachikian, & D. Weedman, IAU Symp., 194, 46
Baan, W. A., & Haschick, A. D. 1987, ApJ, 318, 139
Baan, W. A., & Klöckner, H. R. 2001, in The Central Kiloparsec of Starbursts and AGN: The La Palma Connection, eds. J. H. Knapen, J. E. Beckman, I. Shlosman, & T. J. Mahoney, ASP Conf. Ser., 249, 639
Baan, W. A., Wood, P. A. D., & Haschick, A. D. 1982, ApJ, 260, L49
Baan, W. A., Haschick, A. D., & Henkel, C. 1989, ApJ, 346, 680
Baan, W. A., Haschick, A., & Henkel, C. 1992a, AJ, 103, 728
Baan, W. A., Rhoads, J., Fisher, K., Altschuler, D. R., & Haschick, A. 1992b, ApJ, 396, L99
Briggs, F. H. 1998, A&A, 336, 815
Buat, V., Takeuchi, T. T., Iglesias-Páramo, J., et al. 2007, ApJS, 173, 404
Chambers, K. C., Magnier, E. A., Metcalfe, N., et al. 2016, ArXiv e-prints [arXiv:1612.05560]
Chengalur, J. N., & Kanekar, N. 2003, Phys. Rev. Lett., 91, 241302
Clements, D. L., Sutherland, W. J., McMahon, R. G., & Saunders, W. 1996, MNRAS, 279, 477
Cluver, M. E., Jarrett, T. H., Hopkins, A. M., et al. 2014, ApJ, 782, 90
Cluver, M. E., Jarrett, T. H., Dale, D. A., et al. 2017, ApJ, 850, 68
Darling, J. 2003, Phys. Rev. Lett., 91, 011301
Darling, J. 2004, ApJ, 612, 58
Darling, J. 2007, ApJ, 669, L9
Darling, J., & Giovanelli, R. 2001, AJ, 121, 1278
Darling, J., & Giovanelli, R. 2002, AJ, 124, 100
Farrah, D., Rowan-Robinson, M., Oliver, S., et al. 2001, MNRAS, 326, 1333
Fernandez, M. X., Momjian, E., Salter, C. J., & Ghosh, T. 2010, AJ, 139, 2066
Flambaum, V. V., & Kozlov, M. G. 2007, Phys. Rev. Lett., 98, 240801
Frayer, D. T., Seaquist, E. R., & Frail, D. A. 1998, AJ, 115, 559
Gupta, N., Jagannathan, P., Srianand, R., et al. 2020, ApJ, 907, 11
Hao, C.-N., Kennicutt, R. C., Johnson, B. D., et al. 2011, ApJ, 741, 124
Haynes, M. P., Giovanelli, R., Kent, B. R., et al. 2018, ApJ, 861, 49
Henkel, C., Baan, W. A., & Mauersberger, R. 1991, A&ARv, 3, 47
Houck, J. R., Schneider, D. P., Danielson, G. E., et al. 1985, ApJ, 290, L5
Jansen, P., Xu, L.-H., Kleiner, I., Ubachs, W., & Bethlem, H. L. 2011, Phys. Rev. Lett., 106, 100801
Jarrett, T. H., Cluver, M. E., Brown, M. J. I., et al. 2019, ApJS, 245, 25
Kanekar, N., Carilli, C. L., Langston, G. I., et al. 2005, Phys. Rev. Lett., 95, 261301
Kanekar, N., Langston, G. I., Stocke, J. T., Carilli, C. L., & Menten, K. M. 2012, ApJ, 746, L16
Kanekar, N., Ghosh, T., & Chengalur, J. N. 2018, Phys. Rev. Lett., 120, 061302
Kennicutt, R. C., & Evans, N. J. 2012, ARA&A, 50, 531
Koribalski, B. S., Staveley-Smith, L., Westmeier, T., et al. 2020, Ap&SS, 365, 118
Lo, K. Y. 2005, ARA&A, 43, 625
Lockett, P., & Elitzur, M. 2008, ApJ, 677, 985
Lonsdale, C. J. 2002, in Cosmic Masers: From Proto-Stars to Black Holes, eds. V. Migenes, & M. J. Reid, IAU Symp., 206, 413
Lotz, J. M., Jonsson, P., Cox, T. J., et al. 2011, ApJ, 742, 1
McBride, J., Heiles, C., & Elitzur, M. 2013, ApJ, 774, 35
McKean, J., & Roy, A. L. 2009, Panoramic Radio Astronomy: Wide-field 1–2 GHz Research on Galaxy Evolution, 60
Moshir, M., et al. 1990, IRAS Faint Source Catalogue
Murphy, E. J., Condon, J. J., Schinnerer, E., et al. 2011, ApJ, 737, 67
Norris, R. P., Gardner, F. F., Whiteoak, J. B., Allen, D. A., & Roche, P. F. 1989, MNRAS, 237, 673
Parra, R., Conway, J. E., Elitzur, M., & Pihlström, Y. M. 2005, A&A, 443, 383
Radford, H. E. 1964, Phys. Rev. Lett., 13, 534
Roberts, H., Darling, J., & Baker, A. J. 2021, ApJ, submitted
Robinson, B. J., & McGee, R. X. 1967, ARA&A, 5, 183
Sanders, D. B., & Mirabel, I. F. 1996, ARA&A, 34, 749
Sault, R. J., Teuben, P. J., & Wright, M. C. H. 1995, in Astronomical Data Analysis Software and Systems IV, eds. R. A. Shaw, H. E. Payne, & J. J. E. Hayes, ASP Conf. Ser., 77, 433
Sault, R. J., Teuben, P., & Wright, M. C. H. 2011, MIRIAD: Multi-channel Image Reconstruction, Image Analysis, and Display, Astrophys. Source Code Libr. [record ascl:1106.007]
Schulz, R., Dijkema, T. J., & Molenaar, G. 2020, Apercal: Pipeline for the Westerbork Synthesis Radio Telescope Apertif upgrade, Astrophys. Source Code Libr. [record ascl:2002.010]
Seaquist, E. R., Frayer, D. T., & Frail, D. A. 1997, ApJ, 487, L131
Serra, P., Westmeier, T., Giese, N., et al. 2015, MNRAS, 448, 1922
Skinner, C. J., Smith, H. A., Sturm, E., et al. 1997, Nature, 386, 472
Staveley-Smith, L., Allen, D. A., Chapman, J. M., Norris, R. P., & Whiteoak, J. B. 1989, Nature, 337, 625
Staveley-Smith, L., Norris, R. P., Chapman, J. M., et al. 1992, MNRAS, 258, 725
Suess, K. A., Darling, J., Haynes, M. P., & Giovanelli, R. 2016, MNRAS, 459, 220
Varshalovich, D. A., & Potekhin, A. Y. 1995, Space Sci. Rev., 74, 259
Virtanen, P., Gommers, R., Oliphant, T. E., et al. 2020, Nat. Methods, 17, 261
Webb, J. K., Murphy, M. T., Flambaum, V. V., et al. 2001, Phys. Rev. Lett., 87, 091301
Willett, K. W. 2012, in Cosmic Masers - from OH to H0, eds. R. S. Booth, W. H. T. Vlemmings, & E. M. L. Humphreys, IAU Symp., 287, 345
Willett, K. W., Darling, J., Spoon, H. W. W., Charmandaris, V., & Armus, L. 2011, ApJ, 730, 56
Zhang, J. S., Wang, J. Z., Di, G. X., et al. 2014, A&A, 570, A110

Appendix A: Reliability of the 1612 MHz line

A.1. Matched filter

In order to test the reliability of the 1612 MHz detection, we performed a test using matched filtering. Here we present the matched filtering results on the full spectral resolution (unsmoothed) data; however, we also performed the exact same tests on the smoothed data presented in this work and found the resulting plots to be essentially identical.

The shape of the 1612 MHz line is not known a priori; however, we started with the assumption that the line shapes are approximately the same for all the OH maser lines. This implies that all lines trace the same gas components, although in practice that may not be the case. We took the 1667 MHz profile over the channel range indicated in Fig. 1, and reproduced in Fig. A.1, as an initial guess for the matched filter and applied it using `scipy.signal.filtfilt` (Virtanen et al. 2020). To check the implementation, we first applied the matched filter to the 1667 and 1665 MHz line spectrum. The signal-to-noise is maximized exactly where the 1667 MHz line is detected, as expected, although we note that the 1665 MHz signal is strongly blended with the 1667 MHz signal (blue line in Panel B of Fig. A.1).

We attempted to improve on this by truncating the matched filter at the estimated width of the 1612 MHz line (the line center ±8 channels corresponding to the gray shaded region of Fig. A.1). When we applied the truncated matched filter to the 1665 and 1667 MHz spectrum (black line in Fig. A.1), the 1665 MHz signal became distinct and its peak was also very well localized with the predicted frequency of the 1665 MHz line.

Panel D of Fig. A.1 shows the result of cross-correlating the full matched filter with the 1612 MHz spectrum. The most significant feature, positive or negative, is associated with where we expect the redshift 1612 MHz line to fall. (The rise at the lowest frequencies is an edge effect.) In fact, using the entire 1667 MHz profile for the matched filter may be too broad: while this filter maximizes the S/N, its localization is poor.

Panel E of Fig. A.1 shows the cross-correlation of the 1612 MHz spectrum with this truncated matched filter. The strongest overall feature in the matched filter correlation is negative, and its profile shape appears noise-like. The strongest positive feature is still associated with where we expect the 1612 MHz line to fall, but now the localization is significantly better and remarkably well aligned with the predicted position of the 1612 MHz line. The shape of this positive feature also appears qualitatively different than those of the noise features around it.

Finally, we repeated the work described above with a Gaussian kernel fit to the 1667 MHz profile and a truncated Gaussian profile, which is simply the peak of the same Gaussian now restricted to the inner ±8 channels. We find that the results for the full Gaussian are exactly the same as for the full matched filter. For the truncated Gaussian, the very small (channel by channel) variations seen in Panel E are smoothed out, but it does not change the large-scale variations seen in the plot, or our results.

What we conclude from the six combinations of applying a full matched filter, truncated matched filter, or Gaussian filter to both the full resolution and the smoothed pixel spectra is that the exact shape of the filter does not matter in terms of identifying the most significant features in the spectra. However, the width of the filter is important in localizing these features (e.g., Panel B). Panel (E) is suggestive that there is emission detected from the 1612 MHz line, but the conclusions are tentative and the measurement is still dominated by noise.

A.2. FLASHfinder

We performed a second test using the Bayesian line fitting tool FLASHfinder[8] (Allison et al. 2012, 2014) with a strong redshift constraint. As with the matched filter, the tool was tested on the 1665 and 1667 MHz spectrum, in this case either assuming two Gaussian components or assuming three Gaussian components with redshift priors of $z_\odot = 0.19612 \pm 0.01$. The three-component Gaussian was overwhelmingly favored with a difference in log probability of 17.61 ± 0.07 in order to fit the double peak in the 1667MHz line.

FLASHfinder was then run on the 1612 MHz spectrum with an even stronger redshift prior of $z_\odot = 0.19612 \pm 0.001$. This corresponds to an error of $\sim 300\,\mathrm{km\,s^{-1}}$, although the error in the redshift uncertainty measured by SoFiA for the 1667 MHz line is only $1\,\mathrm{km\,s^{-1}}$. Unfortunately, the Bayesian tool disfavors a Gaussian component at the predicted location of the 1612 MHz line with a log probability of −0.27. More optimistically phrased, the log probability estimates that there is a roughly one in three chance that we have detected the spectral line.

As a result of both the matched filter and the Bayesian analysis, we took the conservative approach throughout the paper of calling the 1612 MHz line measurement an upper limit rather than a tentative detection.

[8] https://github.com/drjamesallison/flash_finder

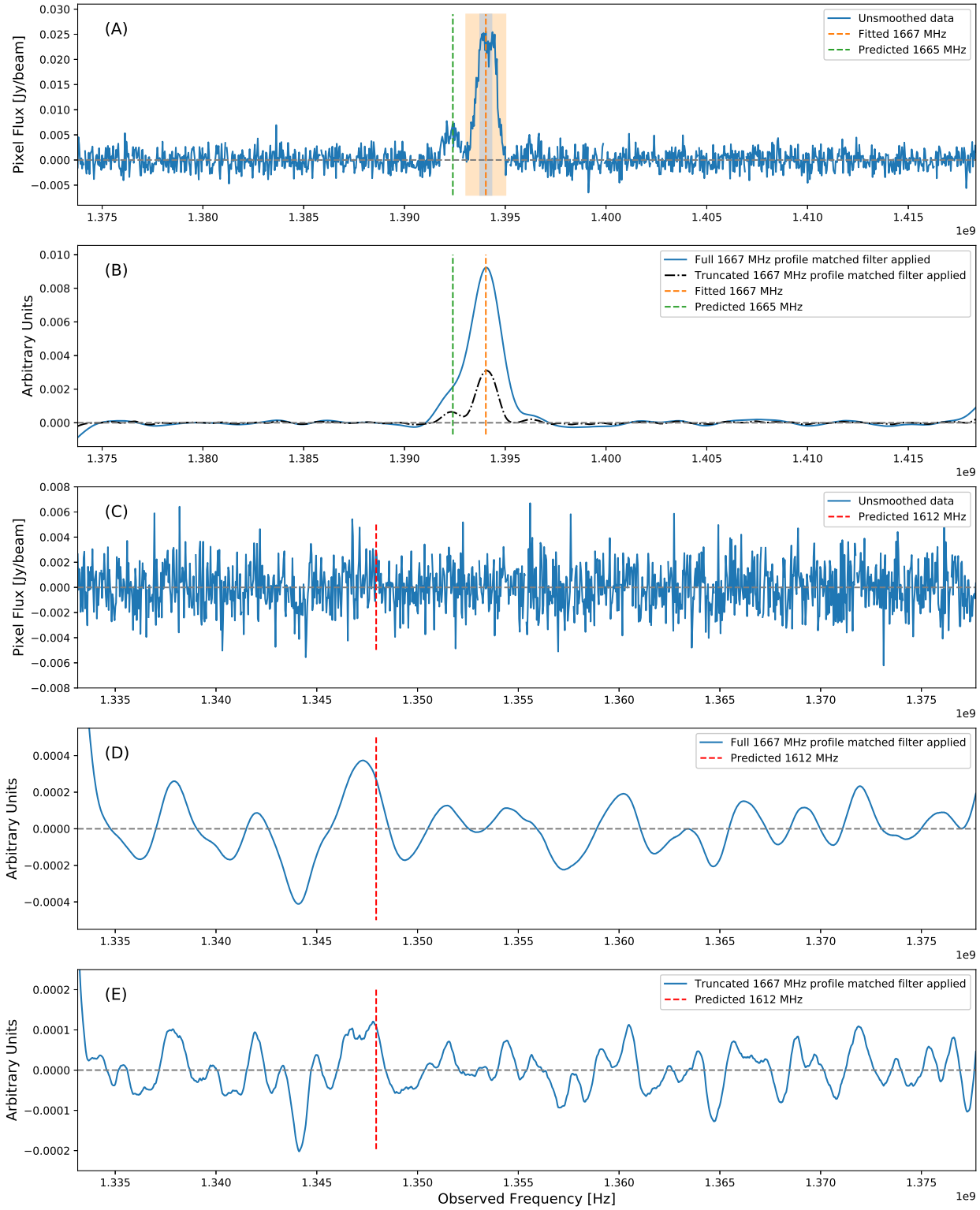

Fig. A.1. Summary of the matched filter tests. *Panel A*: the full resolution (unsmoothed) pixel spectrum showing the 1665 and 1667 MHz lines. The orange shaded region shows the extent of the OH 1667 MHz profile for the full matched filter. The gray shaded region shows the extent of the OH 1667 MHz profile that has been used for the truncated filter. It matches the width over which the 1612 MHz line was measured in Sect. 3. *Panel B*: the matched filters applied to the unsmoothed data. *Panel C*: the full resolution pixel spectrum covering the predicted frequency of the 1612 MHz line. *Panel D*: the full 1667 profile matched filter applied to the unsmoothed 1612 MHz data. *Panel E*: the truncated 1667 MHz profile matched filter applied to the unsmoothed 1612 MHz data.